

Magnetoelectric properties of the multiferroic CuCrO_2 studied by means of *ab initio* calculations and Monte Carlo simulations

Ahmed Albaalbaky,^{1,*} Yaroslav Kvashnin,² Denis Ledue,¹ Renaud Patte,¹ and Raymond Frésard³

¹Normandie Université, UNIROUEN, INSA Rouen,
CNRS, GPM, 76800 Saint Étienne du Rowray, France

²Department of Physics and Astronomy, Division of Materials Theory,
Uppsala University, Box 516, SE-75120 Uppsala, Sweden

³Normandie Université, UNICAEN, ENSICAEN, CNRS, CRISMAT, 14050 Caen, France

(Dated: November 19, 2021)

Motivated by the discovery of multiferroicity in the geometrically frustrated triangular antiferromagnet CuCrO_2 below its Néel temperature T_N , we investigate its magnetic and ferroelectric properties using *ab initio* calculations and Monte Carlo simulations. Exchange interactions up to the third nearest neighbors in the *ab* plane, inter-layer interaction and single ion anisotropy constants in CuCrO_2 are estimated by series of density functional theory calculations. In particular, our results evidence a hard axis along the [110] direction due to the lattice distortion that takes place along this direction below T_N . Our Monte Carlo simulations indicate that the system possesses a Néel temperature $T_N \approx 27$ K very close to the ones reported experimentally ($T_N = 24 - 26$ K). Also we show that the ground state is a proper-screw magnetic configuration with an incommensurate propagation vector pointing along the [110] direction. Moreover, our work reports the emergence of spin helicity below T_N which leads to ferroelectricity in the extended inverse Dzyaloshinskii-Moriya model. We confirm the electric control of spin helicity by simulating *P-E* hysteresis loops at various temperatures.

I. INTRODUCTION

Through the discovery of the mineral CuFeO_2 in 1873, Friedel opened the door to the delafossites ABO_2 [1, 2]. Such a family crystallizes in the layered $R\bar{3}m$ space group, see Fig. 1. The diversity of properties they exhibit raises up an ever increasing interest in this class of compounds. In particular, the discovery of simultaneous transparency and *p*-type conductivity in CuAlO_2 by Kawazoe *et al.* [3], laid ground for the development of transparent optoelectronic devices. Furthermore, depending on the chemical composition, a plethora of behaviors can be evidenced. For instance, for A in a d^9 configuration, e.g., A = Pd or Pt, highly metallic compounds with anomalous temperature dependence of the resistivity have been reported [4–7]. The transport in these compounds has been found to be strongly anisotropic, with a degree of anisotropy that may reach 1000 [4, 5, 8]. For A in a d^{10} configuration, the semi-conducting materials CuBO_2 , with B = Cr, Fe, Rh, may be turned into promising thermoelectric ones through hole doping [9–11] — in particular, an especially high power factor has been found in the case of $\text{CuRh}_{1-x}\text{Mg}_x\text{O}_2$ [12], which transport coefficients served as a basis for the Apparent Fermi Liquid scenario [13]. Regarding the magnetic compounds CuFeO_2 and CuCrO_2 , many studies point towards a strong coupling of the magnetic and structural degrees of freedom [14–22], that paves the way to multiferroelectricity.

With its frustrated triangular lattice CuCrO_2 received a lot of attention since it is ferroelectric without applying

magnetic fields or doping upon Cr^{3+} sites, unlike CuFeO_2 [17, 24]. The emergence of ferroelectricity in CuCrO_2 is induced by the proper-screw magnetic ordering below the Néel temperature T_N , and the control of this ferroelectricity by an applied magnetic field is very important for new spin-based device applications. CuCrO_2 forms a rhombohedral lattice where the edge-shared CrO_6 layers are alternatively stacked between Cu^+ layers along the *c*-axis as shown in Fig. 1. Due to the weak inter-layer interaction J_4 (Fig. 2), the material behaves as a quasi-2D magnet, which makes it even more interesting. The magnetic properties of CuCrO_2 have been investigated by neutron diffraction experiments [20, 25–28]. It was

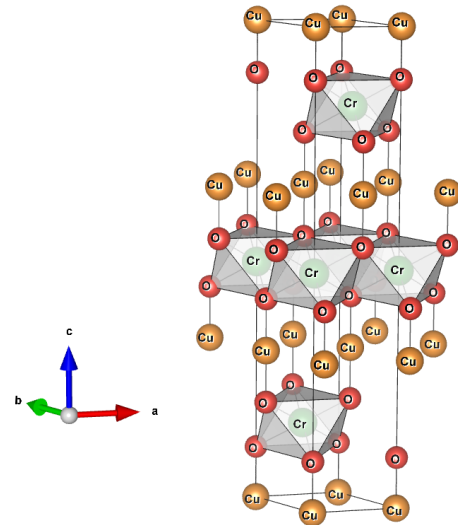


FIG. 1. (Color online) Delafossite structure of CuCrO_2 .

* ahmed.baalbaky@hotmail.com

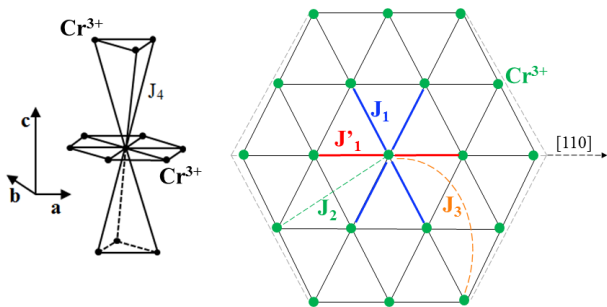


FIG. 2. (Color online) Interlayer and intralayer exchange interactions within an ab plane (blue bonds correspond to J_1 and red bonds correspond to J'_1 with $J_1/J'_1 < 1$).

shown that the magnetic configuration of CuCrO_2 below T_N is proper screw with an incommensurate propagation vector $\mathbf{q} = (0.329, 0.329, 0)$ [28] pointing along the $[110]$ direction. Such deviation from the commensurate magnetic configuration of $\mathbf{q} = (1/3, 1/3, 0)$ is due to the lattice distortion that takes place along the $[110]$ direction below T_N upon the spiral-spin ordering which leads to anisotropic in-plane exchange interactions J_1 and J'_1 (Fig. 2) [29]. Polarized neutron-diffraction measurements on single crystals of CuCrO_2 [20] showed that the spins are oriented in a spiral plane parallel to the (110) plane suggesting that the $[110]$ direction is a hard axis.

The electric polarization emerges upon the spiral-spin ordering [20, 30, 31], which reflects the strong coupling between non-collinear magnetic ordering and ferroelectricity in CuCrO_2 . Within the spin-current model or the inverse Dzyaloshinskii-Moriya (DM) mechanism [32–34], the electric polarization \mathbf{P}_{ij} produced between the canted spins \mathbf{S}_i and \mathbf{S}_j , located at sites i and j , respectively, is given by

$$\mathbf{P}_{ij} \propto \mathbf{e}_{ij} \times (\mathbf{S}_i \times \mathbf{S}_j) \equiv \mathbf{p}_1 \quad (1)$$

where \mathbf{e}_{ij} is a unit vector joining the sites i and j . However, Eq.(1) fails to explain the emergence of ferroelectricity in CuCrO_2 because in the proper-screw configurations, $(\mathbf{S}_i \times \mathbf{S}_j)$ is parallel to \mathbf{e}_{ij} (\mathbf{e}_{ij} is along the $[110]$ direction due to symmetry considerations [30]) unlike the cycloid spin structures.

Based on symmetry considerations, Kaplan and Mahanti [35] introduced an additional contribution $\mathbf{p}_2 \propto (\mathbf{S}_i \times \mathbf{S}_j)$ to the macroscopic polarization which contributes in both cycloid and proper-screw configurations. Therefore, within this model, now referred to as extended DM model, the total polarization is given by

$$\mathbf{P} = \mathbf{p}_1 + \mathbf{p}_2 \quad (2)$$

In this study, we investigate the magnetoelectric properties of CuCrO_2 by means of a combination of Density Functional Theory (DFT) calculations and Monte Carlo (MC) simulations. More precisely, we estimate a set of exchange interactions and anisotropy constants and confront it to the experimental magnetic properties and we

verify the appearance of spiral spin ordering at low temperatures which can be related to the ferroelectric polarization.

In Sec. II we detail briefly the DFT method that we used to extract the coupling and anisotropy constants in CuCrO_2 , while the model and MC method are presented in Sec. III. Sec. IV is devoted to the results where we discuss the magnetic and ferroelectric properties of CuCrO_2 . A conclusion is given in Sec. V.

II. DFT COMPUTATIONAL METHOD

We performed a series of DFT calculations using full-potential linear muffin-tin orbital (FP-LMTO) method as implemented in RSPt [36] code. An experimental crystal structure [37] was considered, taking into account a small in-plane lattice distortion, suggested in Ref. [29]. Our results are in-line with earlier calculations [21]. The DFT+ U [38] approach was used in order to take into account the effect of strong correlations between Cr $3d$ electrons. The adopted values of Hubbard U and Hund's exchange J were 2.3 and 0.96 eV, which were extracted from first-principles calculations for a similar system LiCrO_2 [23]. The same computational scheme was used in a prior study on the magnetic properties of CuCrO_2 [22]. The Fully Localized Limit (FLL) [39] formed of the double-counting correction was applied. We calculated the exchange parameters between Cr^{3+} ions by means of the magnetic force theorem [40, 41]. The so-called muffin-tin head projection scheme was applied to construct the set of localized Cr- d orbitals (for more details see Ref. [42]). The J_{ij} 's were extracted from both ferromagnetic and antiferromagnetic configurations. The obtained values turned out to be insensitive to the assumed magnetic order, which implies that they can be used as fixed parameters in a Hamiltonian describing the interacting spins. The spin-orbit coupling was taken into account only for the calculation of the magnetocrystalline anisotropy, which was calculated directly from the total energies.

III. MODEL AND MONTE CARLO SIMULATION

To model the magnetic properties of CuCrO_2 , we note that Cr^{3+} ions with $S = 3/2$ spins are large enough to be treated classically, so we used the following classical three dimensional (3D) Heisenberg Hamiltonian

$$H = - \sum_{\langle i,j \rangle} J_{ij} \mathbf{S}_i \cdot \mathbf{S}_j - D_x \sum_i S_{ix}^2 - D_z \sum_i S_{iz}^2 + g\mu_B \mathbf{B} \cdot \sum_i \mathbf{S}_i \quad (3)$$

where J_{ij} refers to the exchange interactions up to the 4th neighbors (Fig. 2). The x -axis corresponds to the

[110] direction and the z -axis corresponds to the [001] direction. $D_x < 0$ and $D_z > 0$ correspond to the hard and easy axes anisotropy constants respectively. The fourth term corresponds to the Zeeman energy where \mathbf{B} is the applied magnetic field (μ_B is the Bohr magneton and $g = 2$ is the Landé factor).

To model the ferroelectric properties of CuCrO_2 and the coupling between the spins and the electric field \mathbf{E} , we added the following term to the previous Hamiltonian

$$H_e = -A_0 \mathbf{E} \cdot \sum_{\langle i,j \rangle} \mathbf{S}_i \times \mathbf{S}_j \quad (4)$$

where the sum runs over the magnetic bonds along the [110] direction, and A_0 is a coupling constant related to the spin-orbit and spin exchange interactions. Adding this contribution leads to the model for multiferroics proposed by Kaplan and Mahanti [35].

Our MC simulations [43] were performed on 3D triangular lattices (Fig. 1 with only Cr^{3+} ions) with periodic boundary conditions (PBC) using the standard Metropolis algorithm [44] and the time-step-quantified method [45] when needed.

Typically, the first 2×10^4 MC steps were discarded for thermal equilibration before averaging over the next 3×10^5 MC steps. Note that our results are averaged over 24 simulations with different random number sequences so that statistical fluctuations are negligible.

IV. RESULTS AND DISCUSSIONS

It was reported in Ref. [29] that the lattice undergoes a tiny in-plane distortion $d = (a_2 - a_1)/a_1$ below T_N with a_1 and a_2 being the lattice constants along the [110] and the [100] directions, respectively. As a first step, we considered $d = 0.0001$ [29] to calculate the exchange interactions and anisotropy constants in CuCrO_2 . The extracted values given in Table I (line 1) are very close to the ones reported in Ref. [46] concerning J_1 and J'_1 as well as the single ion anisotropy constants. Note that here J_1/J'_1 is very close to 1 ($J_1/J'_1 = 0.995$). Knowing that PBC favors the commensurate configuration when J_1/J'_1 is close to 1, large enough sizes are required to obtain an incommensurate magnetic ground state (GS). However, a MC simulation with $90 \times 90 \times 2$ unit cells was not able to reproduce an incommensurate GS with this set of

TABLE I. Estimated DFT values of the exchange interactions and anisotropy constants (in meV). More precisely, for $d=0.0001$, the calculated value of D_x was smaller than 10^{-4} meV, which is negligible.

d	J'_1	J_1	J_2	J_3	J_4	D_x	D_z
0.0001	-2.419	-2.407	0.012	-0.266	-0.060	0.000	0.033
0.003	-2.709	-2.383	0.012	-0.266	-0.060	-0.001	0.033

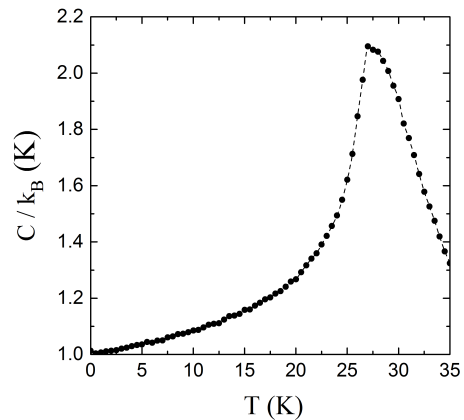


FIG. 3. Simulated temperature dependence of the specific heat per spin of CuCrO_2 . The parameter values are given in Table I for $d=0.003$.

interactions ($d = 0.0001$). Thus larger sizes of the simulation box were required which are not accessible within reasonable computer time [47]. Therefore we enhanced the lattice distortion by a factor of 30 (i.e. $d = 0.003$). We found that the new set of J_{ij} 's ($J_1/J'_1 = 0.88$) and anisotropy constants (Table I) is a good candidate to reproduce an incommensurate GS for a system of reasonable size $45 \times 45 \times 2$ unit cells. It is worth noting that the considered distortion mainly affect the first nearest neighbors interactions while the remaining interactions are not affected. Also it is very interesting to note that the magnitude of the in-plane anisotropy constant (D_x) increases when enhancing the lattice distortion reflecting that this anisotropy results from the lattice distortion.

A. Magnetic properties

In order to characterize the GS configuration and to estimate the Néel temperature T_N we performed a first set of simulations without applying an external magnetic field. The following procedure has been retained: we started the simulations from random spin configurations at a high enough temperature ($T > T_N$) and we then cooled down to $T_{\text{final}} = 0.01$ K with a constant temperature step $\Delta T = 0.5$ K.

In order to estimate the Néel temperature, we calculated the specific heat per spin defined as

$$C = \frac{1}{N} \frac{\partial U}{\partial T} = \frac{\langle E^2 \rangle_T - \langle E \rangle_T^2}{N k_B T^2} \quad (5)$$

where $U(T) = \langle E \rangle_T$ with E being the energy of each magnetic configuration, $\langle \dots \rangle_T$ means thermal average, N is the number of spins and k_B is the Boltzmann constant. For the parameter set given in Table I ($d = 0.003$) the phase transition as signaled by the peak of the specific heat (Fig. 3) takes place at $T_N = 27.0 \pm 0.5$ K. This value is in a good agreement with the reported experimental values ($T_N = 24 - 26$ K) [9, 28, 30]. This may

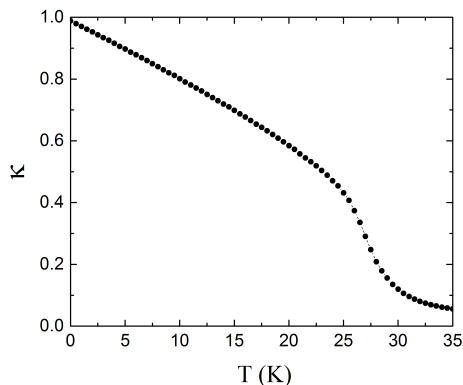


FIG. 4. Simulated temperature dependence of the order parameter in CuCrO_2 (at $T \approx 0$ K, $\kappa \approx 0.988$).

be taken as a first validation of the extracted exchange interactions of Table I.

To characterize the nearly 120° GS configuration we considered the spin chirality defined as

$$\kappa_p = \frac{1}{S^2} \frac{2}{3\sqrt{3}} (\mathbf{S}_1 \times \mathbf{S}_2 + \mathbf{S}_2 \times \mathbf{S}_3 + \mathbf{S}_3 \times \mathbf{S}_1) \quad (6)$$

where 1, 2 and 3 refer to the spins at the corners of each elementary triangular plaquette p in an ab plane. Then we defined the order parameter per plane to be $\lambda = \frac{1}{n_p} \|\sum_p \kappa_p\|$ where n_p is the number of plaquettes per plane, and finally the order parameter of the whole system was defined as $\kappa = \langle \bar{\lambda} \rangle_T$ where $\bar{\lambda}$ is the average of λ over the ab planes. We found that the direction of the vector chirality ($\boldsymbol{\lambda}$) of each ab plane is pointing along the $[110]$ direction confirming the fact that the spins are oriented in the (110) plane as reported in Ref. [20]. Fig. 4 shows the variation of the order parameter as function of temperature. At $T \approx 0$ K, $\kappa \approx 0.988$ indicates a small deviation from the commensurate (120°) configuration of $\kappa = 1$. Moreover, the simulated value of $\mathbf{q} \approx (0.322, 0.322, 0)$ confirms that the GS is an incommen-

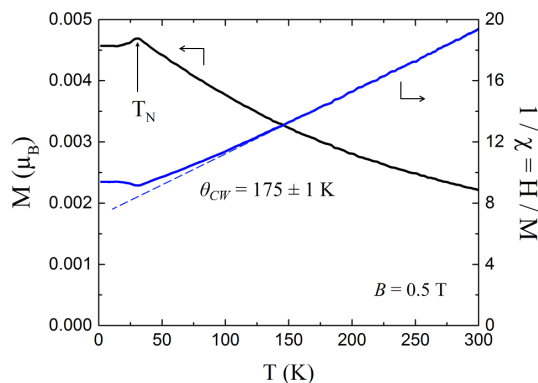


FIG. 5. (Color online) Simulated temperature dependence of the magnetization per spin and the inverse susceptibility under $B = 0.5$ T magnetic field in CuCrO_2 .

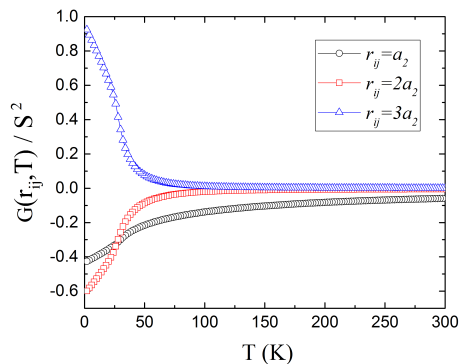


FIG. 6. (Color online) Simulated temperature dependence of the spin-spin correlation functions along $[100]$ calculated at distances a_2 (black circles), $2a_2$ (red squares) and $3a_2$ (blue triangles) in CuCrO_2 .

surate configuration very close to the reported experimental configuration of $\mathbf{q} = (0.329, 0.329, 0)$ [28]. This good agreement may be taken as another validation of the parameters of Table I.

On the other hand, the magnetic field dependence of the magnetization calculated along the easy axis (z -axis) shows a linear behavior (-5 T $< H_z < 5$ T) confirming the antiferromagnetic nature of the GS (not shown here).

Magnetic properties under 0.5 T were simulated between 300 K and 2 K to estimate the Curie-Weiss temperature (θ_{CW}). Fig. 5 shows the variation of the magnetization and inverse susceptibility measured along the applied magnetic field. It can be seen that $1/\chi$ obeys well the Curie-Weiss law for antiferromagnets ($1/\chi = (T + \theta_{CW})/C$, with C is the Curie constant) at high temperatures with $\theta_{CW} = 175 \pm 1$ K close to the measured experimental values ($\theta_{CW} = 160 - 170$ K) [9, 48]. The $1/\chi$ curve starts to deviate from the linear behavior at about 100 K. In order to understand the origin of this deviation we calculated the temperature dependence of the spin-spin correlation function defined as $G(r_{ij}, T) = \langle \mathbf{S}_i \cdot \mathbf{S}_j \rangle_T$ along the $[100]$ direction. As shown in Fig. 6, short-range antiferromagnetic correlations start to develop below ~ 100 K, which leads to the deviation from the Curie-Weiss law seen in Fig. 5. Furthermore, these correlation functions exhibit inflection points close to T_N estimated from the specific heat curve (Fig. 3). Besides, an anomaly in the magnetization curve (Fig. 5) appears at 28 ± 2 K consistent with the estimate of T_N from the specific heat curve. We note that the ratio $\theta_{CW}/T_N \approx 6.5 (\gg 1)$ reflects the frustrated nature of the GS [49, 50].

B. Ferroelectric properties

In this section, we considered the Hamiltonian $H + H_e$. In these simulations, we applied a poling electric field during the cooling process to obtain a single ferroelectric domain. We then turned it off just before statisti-

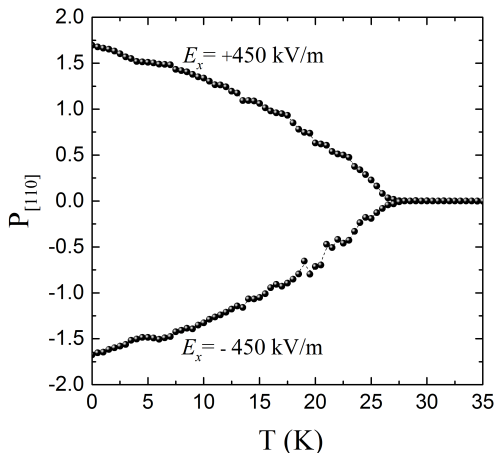


FIG. 7. Simulated temperature dependence of the electric polarization \mathbf{P} calculated along the [110] direction in CuCrO_2 .

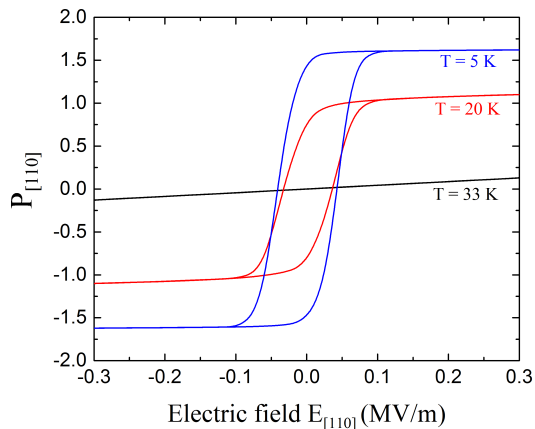


FIG. 8. (Color online) P - E hysteresis loops simulated at different temperatures in CuCrO_2 .

cal averaging to calculate \mathbf{p}_2 which is associated to the spontaneous ferroelectric polarization (Eq. (2)) according to Ref. [35]. Fig. 7 shows the temperature dependence of $P_{[110]}$, the projection of \mathbf{p}_2 along the [110] direction, which starts to develop at T_N . It is clearly seen that by switching the poling electric field, $P_{[110]}$ can be reversed.

Further insight into the degree of electrical polarization may be gained through the knowledge of the P - E hysteresis loops, which are shown in Fig. 8 at different temperatures. $P_{[110]}$ shows a linear E dependence without hysteresis above T_N because the system is in the paraelectric phase, while clear hysteresis loops are seen for temperatures below T_N . This strongly suggests

that ferroelectricity is induced by the out-of-plane incommensurate magnetic configuration, in agreement with Ref. [31]. Also, it can be seen that below T_N the saturation field $E_{sat} \approx 8.9 \times 10^{-2}$ MV/m is independent of the temperature. The hysteresis loop simulated at 5 K shows an electric coercive field for $P_{[110]}$ reversal $E_r \approx 4.2 \times 10^{-2}$ MV/m very close to that measured experimentally ($E_r = 5.1 \times 10^{-2}$ MV/m [51]). Note that the reversal of $P_{[110]}$ results from the reversal of the helicity of each ab atomic plane. Thus our simulations confirm the electric control of spin helicity in CuCrO_2 as reported in Ref. [20].

V. CONCLUSION

In this paper, we proposed estimates of the exchange interactions and single ion anisotropy constants in the multiferroic CuCrO_2 using DFT calculations. They were checked against the experimental Néel and Curie–Weiss temperatures as well as the electric coercive field, thereby proving them to be good candidates to model the magnetoelectric properties of CuCrO_2 . We showed that the lattice distortion that takes place below T_N is responsible for the appearance of a weak in-plane hard-axis anisotropy. Regarding the magnetic properties, we obtained a peak in the specific heat curve at $T_N \approx 27$ K very close to the experimental observations. Furthermore the ground-state has been shown to be an antiferromagnetic incommensurate proper-screw configuration. The estimated $\theta_{CW} \approx 175$ K is in a good agreement with experimental data too. Also, our simulated P - E hysteresis loops confirm the electric control of spin helicity which is related to the ferroelectric polarization below T_N .

ACKNOWLEDGMENTS

We gratefully thank M. Alouani and S. Hébert for stimulating discussions. We are grateful to the Centre Régional Informatique et d'Applications Numériques de Normandie (CRIANN) where our simulations were performed as project number 2015004. We also acknowledge the computational resources provided by the Swedish National Infrastructure for Computing (SNIC) and Uppsala Multidisciplinary Center for Advanced Computational Science (UPPMAX). The authors acknowledge the financial support of the French Agence Nationale de la Recherche (ANR), through the program Investissements d'Avenir (ANR-10-LABX-09-01) and LabEx EMC3.

[1] C. Friedel, *Sciences Academy* **77**, 211 (1873).

[2] R. D. Shannon, D. B. Rogers and C. T. Prewitt, *Inorg. Chem.* **10**, 713 (1971); C. T. Prewitt, R. D. Shannon and D. B. Rogers, *Inorg. Chem.* **10**, 719 (1971); D. B. Rogers,

R. D. Shannon, C. T. Prewitt and J. L. Gillson, *Inorg. Chem.* **10**, 723 (1971).

[3] H. Kawazoe, M. Yasukawa, H. Hyodo, M. Kurita, H. Yanagi, and H. Hosono, *Nature* **389**, 939 (1997).

- [4] H. Takatsu, S. Y. Onezawa, S. M. Ouri, S. Nakatsuji, K. T. Anaka, and Y. Maeno, *J. Phys. Soc. Jpn* **76**, 104701 (2007).
- [5] C. W. Hicks, A. S. Gibbs, A. P. Mackenzie, H. Takatsu, Y. Maeno, and E. A. Yelland, *Phys. Rev. Lett.* **109**, 116401 (2012).
- [6] C. W. Hicks, A. S. Gibbs, L. Zhao, P. Kushwaha, H. Borrmann, A. P. Mackenzie, H. Takatsu, S. Yonezawa, Y. Maeno, and E. A. Yelland, *Phys. Rev. B* **92**, 014425 (2015).
- [7] P. Kushwaha, V. Sunko, P. J. W. Moll, L. Bawden, J. M. Riley, N. Nandi, H. Rosner, M. P. Schmidt, F. Arnold, E. Hassinger, T. K. Kim, M. Hoesch, A. P. Mackenzie, and P. D. C. King, *Science Advances* **1**, 1500692 (2015).
- [8] R. Daou, R. Frésard, S. Hébert, and A. Maignan, *Phys. Rev. B* **91**, 041113(R) (2015).
- [9] T. Okuda, N. Jufuku, S. Hidaka, and N. Terada, *Phys. Rev. B* **72**, 144403 (2005).
- [10] T. Nozaki, K. Hayashi, and T. Kajitani, *J. Chem. Eng. Japn* **40**, 1205 (2007).
- [11] K. Kuriyama, M. Nohara, T. Sasagawa, K. Tabuko, F. Mizokawa, K. Kimura, and H. Takagi, *Proc. 25th Int. Conf. Thermoelectrics* (IEEE, Piscataway, 2006), p. 97.
- [12] A. Maignan, V. Eyert, C. Martin, S. Kremer, R. Frésard, and D. Pelloquin, *Phys. Rev. B* **80**, 115103 (2009).
- [13] S. Kremer and R. Frésard, *Ann. Phys. (Berlin)* **524**, 21 (2012).
- [14] M. Mekata, N. Yaguchi, T. Takagi, S. Mitsuda, and H. Yoshizawa, *J. Magn. Magn. Mater.* **823**, 104 (1992).
- [15] M. Mekata, N. Yaguchi, T. Takagi, T. Sugino, S. Mitsuda, H. Yoshizawa, N. Hosoito, and T. Shinjo, *J. Phys. Soc. Japan* **62**, 4474 (1993).
- [16] O. A. Petrenko, G. Balakrishnan, M. R. Lees, D. McK. Paul, and A. Hoser, *Phys. Rev. B* **62**, 8983 (2000).
- [17] T. Kimura, J. C. Lashley, and A. P. Ramirez, *Phys. Rev. B* **73**, 220401(R) (2006).
- [18] F. Ye, Y. Ren, Q. Huang, J. A. Fernandez-Baca, P. Dai, J. W. Lynn, and T. Kimura, *Phys. Rev. B* **73**, 220404(R) (2006).
- [19] V. Eyert, R. Frésard, and A. Maignan, *Phys. Rev. B* **78**, 052402 (2008).
- [20] M. Soda, K. Kimura, T. Kimura, M. Matsuura, and K. Hirota, *J. Phys. Soc. Jpn.* **78**, 124703 (2009).
- [21] A. Maignan, C. Martin, R. Frésard, V. Eyert, E. Guilmeau, S. Hébert, M. Poienar, and D. Pelloquin, *Solid Stat. Comm.* **149**, 962 (2009).
- [22] J. Xue-Fan, L. Xian-Feng, W. Yin-Zhong, and H. Jiu-Rong, *Chin. Phys. B* **21**, 077502 (2012).
- [23] I. I. Mazin, *Phys. Rev. B* **75**, 094407 (2007).
- [24] J. T. Haraldsen, F. Ye, R. S. Fishman, J. A. Fernandez-Baca, Y. Yamaguchi, K. Kimura, and T. Kimura, *Phys. Rev. B* **82**, 020404(R) (2010).
- [25] H. Kadowaki, H. Kikuchi, and Y. Ajiro, *J. Phys.: Condens. Matter* **2**, 4485 (1990).
- [26] M. Soda, K. Kimura, T. Kimura, and K. Hirota, *Phys. Rev. B* **81**, 100406(R) (2010).
- [27] M. Frontzek, G. Ehlers, A. Podlesnyak, H. Cao, M. Matsuda, O. Zaharko, N. Aliouane, S. Barilo, and S. V. Shiryayev, *J. Phys.: Condens. Matter* **24**, 016004 (2012).
- [28] M. Poienar, F. Damay, C. Martin, V. Hardy, A. Maignan, and G. André, *Phys. Rev. B* **79**, 014412 (2009).
- [29] K. Kimura, T. Otani, H. Nakamura, Y. Wakabayashi, and T. Kimura, *J. Phys. Soc. Jpn.* **78**, 113710 (2009).
- [30] S. Seki, Y. Onose, and Y. Tokura, *Phys. Rev. Lett.* **101**, 067204 (2008).
- [31] K. Kimura, H. Nakamura, K. Ohgushi, and T. Kimura, *Phys. Rev. B* **78**, 140401(R) (2008).
- [32] Y. Tokura and S. Seki, *Adv. Mater.* **22**, 1554 (2010).
- [33] Y. Tokura, S. Seki, and N. Nagaosa, *Rep. Prog. Phys.* **77**, 076501 (2014).
- [34] N. Terada, *J. Phys.: Condens. Matter* **26**, 453202 (2014).
- [35] T. A. Kaplan and S. D. Mahanti, *Phys. Rev. B* **83**, 174432 (2011).
- [36] J. M. Wills, O. Eriksson, M. Alouani, and D. L. Price, in *Electronic Structure and Physical Properties of Solids, Lecture Notes in Physics*, Vol. 535, edited by H. Dreyse (Springer Berlin Heidelberg, 2000) p. 148-167.
- [37] Y. Ono, K. I. Satoh, T. Nozaki, and T. Kajitani, *Jpn. J. Appl. Phys.* **46**, 1071 (2007).
- [38] A. I. Liechtenstein, V. I. Anisimov, and J. Zaanen, *Phys. Rev. B* **52**, R5467(R) (1995).
- [39] M. T. Czyzyk and G. A. Sawatzky, *Phys. Rev. B* **49**, 14211 (1994).
- [40] A. I. Liechtenstein, M. I. Katsnelson, V.P. Antropov, and V. A. Gubanov, *J. Magn. Magn. Mater.* **67**, 65 (1987).
- [41] M. I. Katsnelson and A.I. Lichtenstein, *Phys. Rev. B* **61**, 8906 (2000).
- [42] Y. O. Kvashnin, O. Grånäs, I. Di Marco, M. I. Katsnelson, A. I. Lichtenstein, and O. Eriksson, *Phys. Rev. B* **91**, 125133 (2015).
- [43] D.P. Landau and K. Binder, *A Guide to Monte Carlo Simulations in Statistical Physics* (Cambridge University Press, Cambridge, England, 2008).
- [44] N. Metropolis, A. W. Rosenbluth, M. N. Rosenbluth, A. H. Teller, and E. Teller, *J. Chem. Phys.* **21**, 1087 (1953).
- [45] U. Nowak, R. W. Chantrell, and E. C. Kennedy, *Phys. Rev. Lett.* **84**, 163 (2000).
- [46] H. Yamaguchi, S. Ohtomo, S. Kimura, M. Hagiwara, K. Kimura, T. Kimura, T. Okuda, and K. Kindo, *Phys. Rev. B* **81**, 033104 (2010).
- [47] Note that systems larger than $90 \times 90 \times 2$ unit cells require more than 12.5 days of simulation which is not accessible at the super-computer of CRIANN.
- [48] T. Okuda, R. Kajimoto, M. Okawa, and T. Saitoh, *Int. J. Mod. Phys. B* **27**, 1330002 (2013).
- [49] A. P. Ramirez, *Annu. Rev. Mater. Sci.* **24**, 453 (1994).
- [50] J. E. Greedan, *J. Mater. Chem.* **11**, 37 (2001).
- [51] K. Kimura, H. Nakamura, S. Kimura, M. Hagiwara, and T. Kimura, *Phys. Rev. Lett.* **103**, 107201 (2009).